Supporting Information for:

Tuning the low-temperature phase behavior of aqueous ionic liquids

Authors: Johannes Bachler[1], Isabella Daidone[2], Laura Zanetti-Polzi[3], Thomas Loerting[1,*]

Affiliations:

[1]Institute of Physical Chemistry, University of Innsbruck, Innrain 52c, A-6020 Innsbruck, Austria
[2]Department of Physical and Chemical Sciences, University of L'Aquila, 67010 L'Aquila, Italy
[3]Center S3, CNR-Institute of Nanoscience, 41125 Modena, Italy

* e-mail: thomas.loerting@uibk.ac.at

This document contains the following:

1. Full calorimetry scans recorded for different cooling rates Q_{cool}. The traces in Fig. S3 (Q = 30 K min^{-1}) correspond to the scans of Fig. 2 in the main manuscript for the whole temperature range.
2. A brief summary to the origin of the heat capacity overshoot along the lines of Moynihan and co-workers.[1,2]
3. A summary of the enthalpy differencing procedure promoted by Wang, Velikov and Angell.[3]
4. Behavior of the glass transitions of aqueous ionic liquids studied in this work with changing cooling rate Q_{cool}. This is crucial for the determination of the fragility indices shown in Fig. 3b, c in the main manuscript.
5. Pair radial distribution functions, average hydrogen bond distances and average number of hydrogen bonds as determined from MD simulations of $N_2H_5^+TFA^-$ solution at 300 K.

1. Full calorimetry scans employing different cooling rates Q_{cool}

Panels a in Figs. S1-S6 depicts the whole temperature range of our calorimetry traces of aqueous ionic liquids (and pure glycerol) at solute mole fraction x = 0.175 cooled with Q_{cool} = 100 K min^{-1}, 50 K min^{-1}, 30 K min^{-1}, 10 K min^{-1}, 5 K min^{-1} and 2 K min^{-1}. The drop in baseline starting at 300 K that is present in all cooling scans is not related to sample but corresponds to the transient response of the instrument itself. Similarly, there is an artefact around 140 K for high Q_{cool} scans due to the instrument no longer being able to maintain the high cooling rate. The arguably most interesting observation in the cooling scans is the switch from broad exotherms to narrow exotherms (sometimes also occurring at different temperatures) in many of the aqueous solutions upon decreasing Q_{cool} (see e.g., $N_2H_5^+PFP^-$ in Fig. S1 and Fig. S4). It most likely relates to the change from complex "LLT" behavior to crystallization of ice.

In panel b, the corresponding reheating scans, all with Q_{heat} = 30 K min^{-1}, are shown. First and foremost, it allows identifying the nature ("LLT" or ice crystallization) of exothermic phase transitions observed upon cooling. In the case of crystallization, the warm up traces mostly feature a glass transition of the freeze-concentrated solution followed by cold-crystallization and melting (see, e.g., $C_2H_5NH_3^+TFA^-$ in Fig. S6). In the case of LLT, the behavior is more complex, ranging from endotherms to multiple glass transitions before cold-crystallization and melting (see, e.g., $C_2H_5NH_3^+TFA^-$ in Fig. S1).

In short, the scans presented here show that the complex low-temperature phase behavior of aqueous ionic liquids can be further tuned by varying the cooling rate.

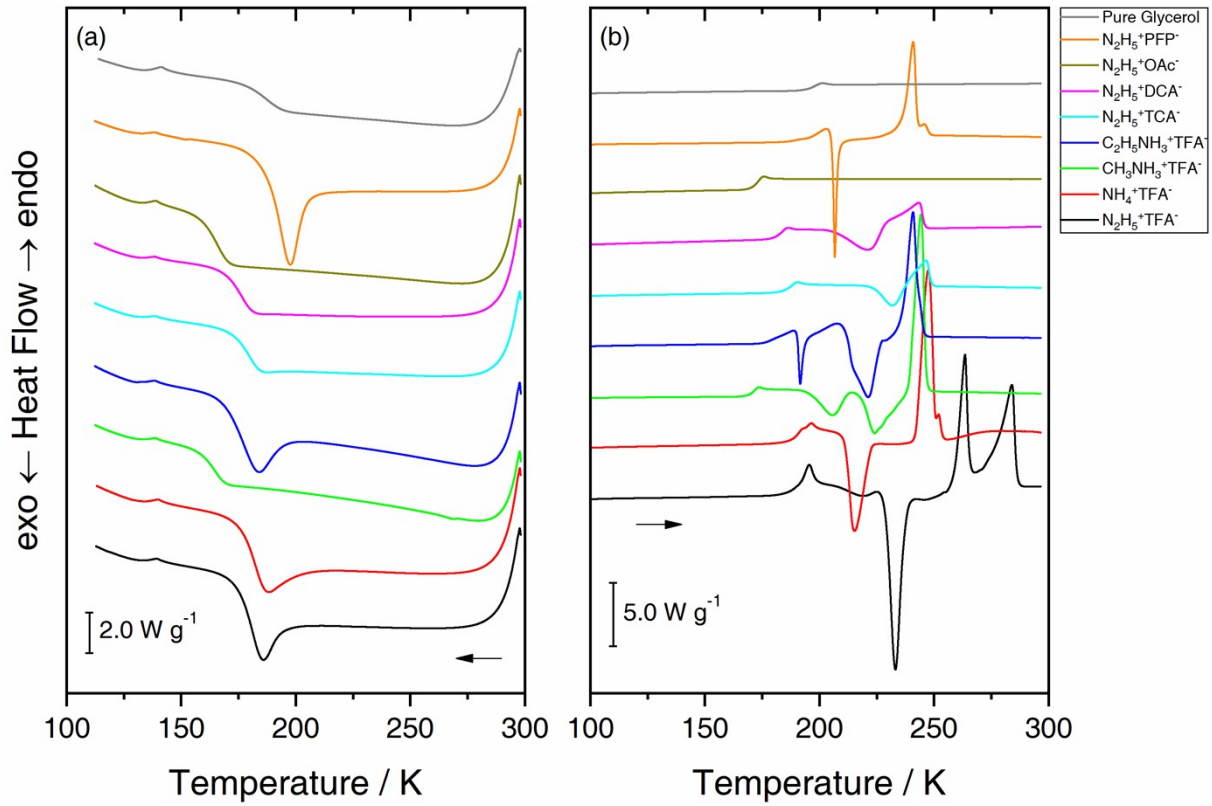

Figure S1. Calorimetry scans of all liquids employed in this work (a) when cooling with 100 K min^{-1} and (b) when reheating with 30 K min^{-1}.

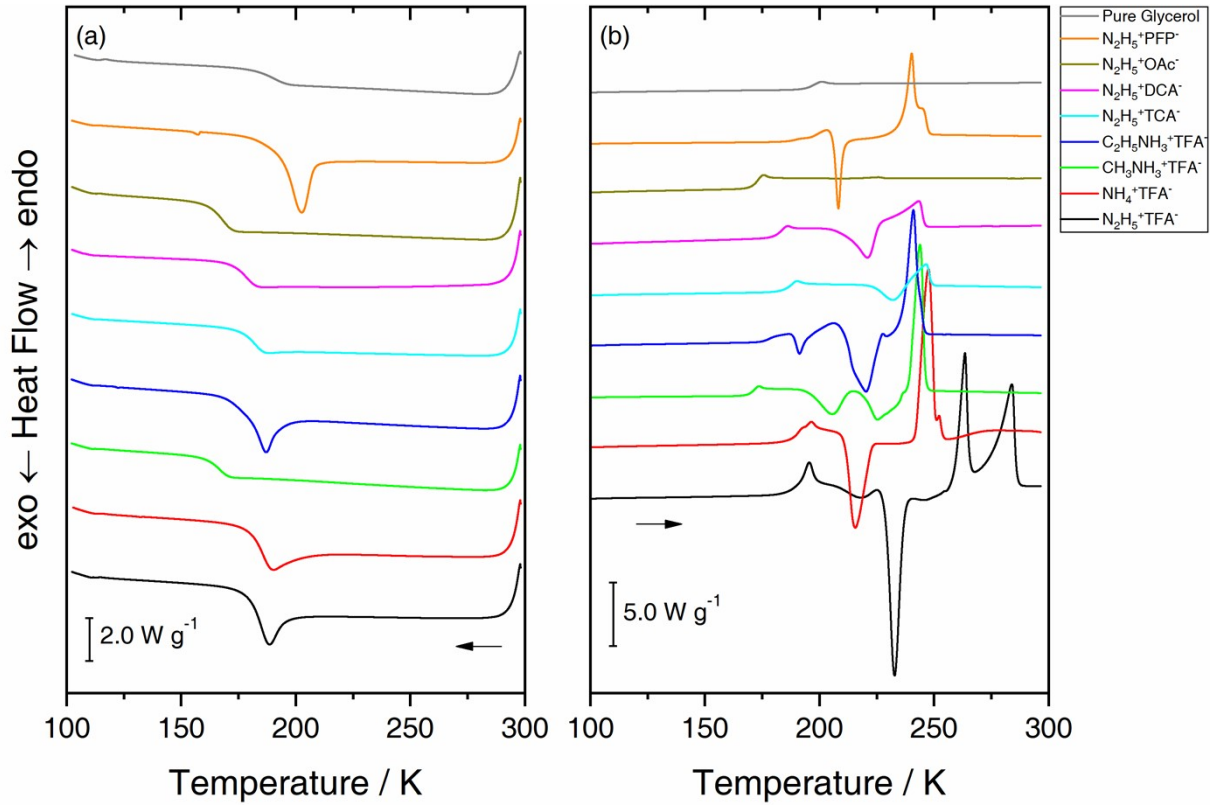

Figure S2. Calorimetry scans of all liquids employed in this work (a) when cooling with 50 K min^{-1} and (b) when reheating with 30 K min^{-1}.

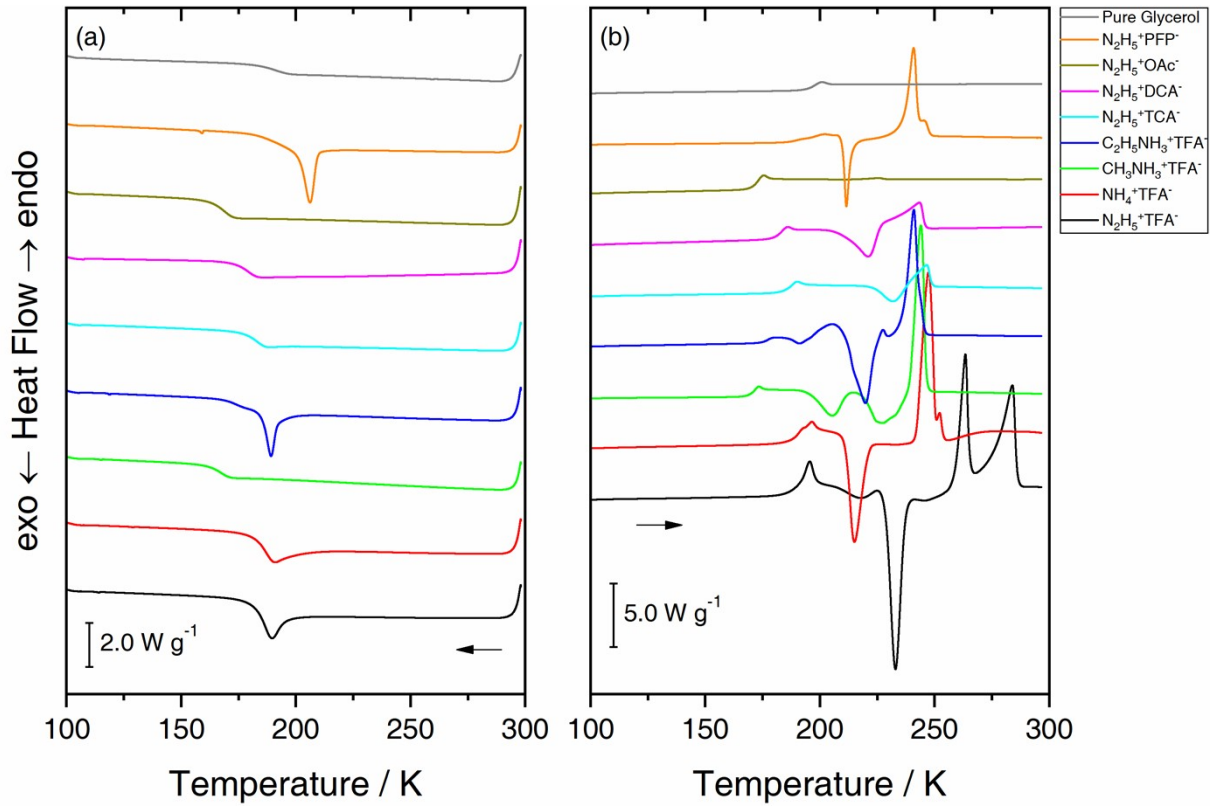

Figure S3. Calorimetry scans of all liquids employed in this work (a) when cooling with 30 K min^{-1} and (b) when reheating with 30 K min^{-1}.

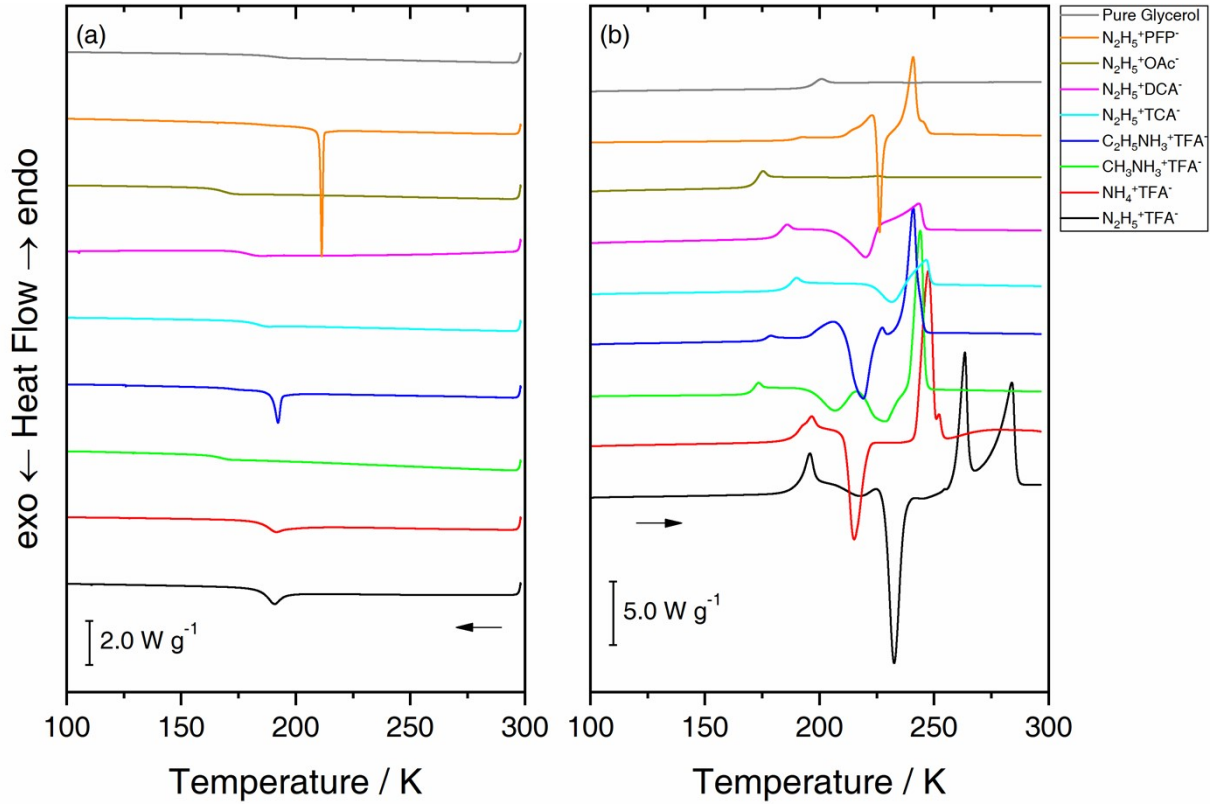

Figure S4. Calorimetry scans of all liquids employed in this work (a) when cooling with 10 K min^{-1} and (b) when reheating with 30 K min^{-1}.

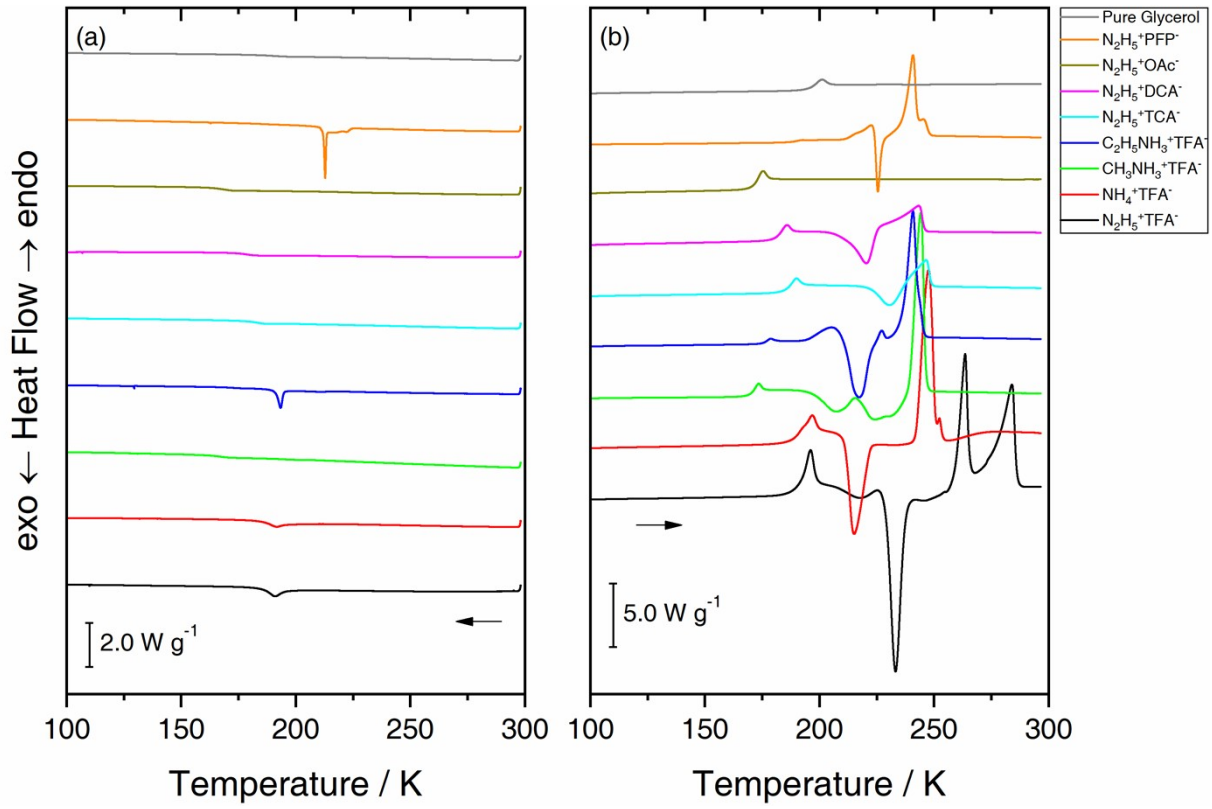

Figure S5. Calorimetry scans of all liquids employed in this work (a) when cooling with 5 K min^{-1} and (b) when reheating with 30 K min^{-1}.

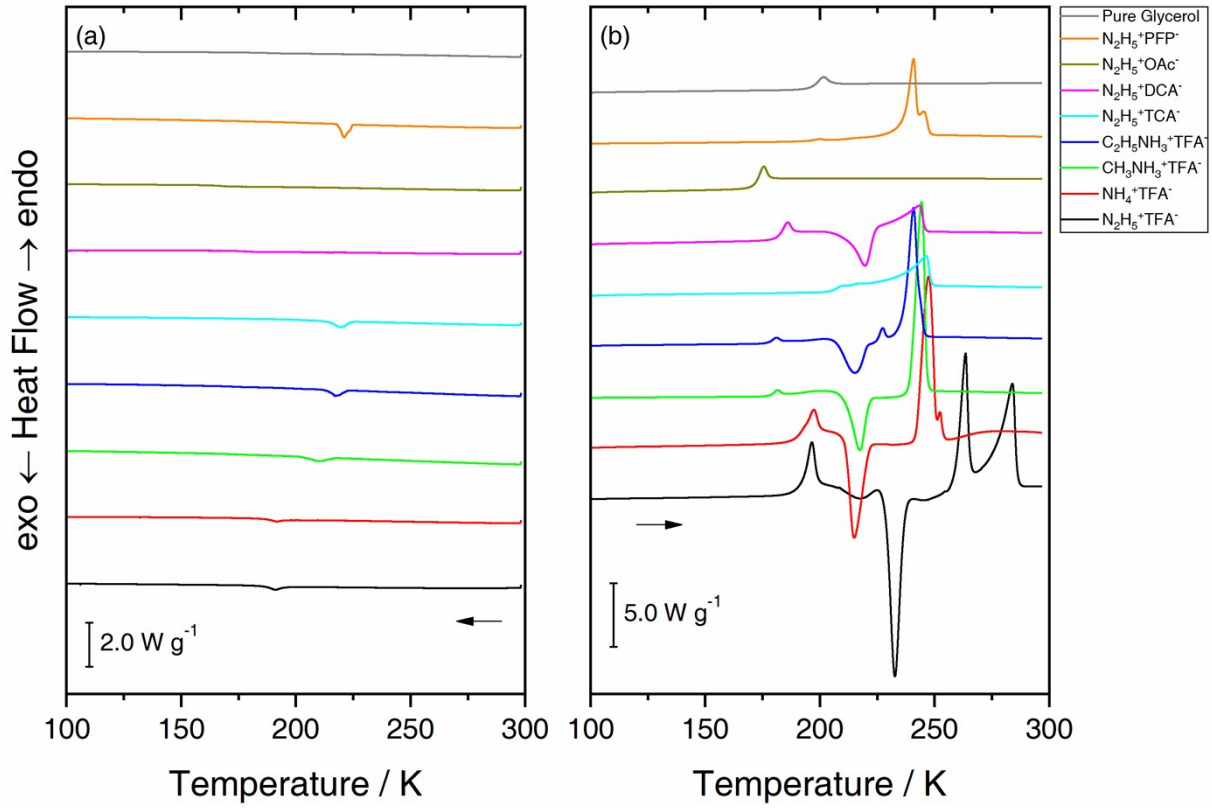

Figure S6. Calorimetry scans of all liquids employed in this work (a) when cooling with 2 K min^{-1} and (b) when reheating with 30 K min^{-1}.

2. Origin of the heat capacity overshoot

In this section, we focus solely on the basics of glass physics that are needed to understand the origin of heat capacity overshoots commonly observed in DSC measurements. For a more detailed discussion on the characteristics of the glass transition in calorimetry, we refer the interested reader to the seminal works by Moynihan and co-workers.[1,2,4]

The most straightforward way to produce glasses is to cool down liquids fast, leaving no time for the formation of crystals (= vitrification). Some liquids require ultrafast cooling to form a glass (e.g., water, $Q > 10^6$ K min^{-1}) whereas others (e.g., glycerol) vitrify easily even with rates lower than 1 K min^{-1}. Upon cooling a liquid, its viscosity (which is proportional to the relaxation time) increases continuously while enthalpy decreases (see Fig. S7 upper panel). This is because the structure of the liquid constantly adapts to the change in temperature. The structural relaxation slows down with decreasing temperature, up to the point where it becomes so slow that it matches the typical timescales of experiments. This rather narrow temperature range termed the transformation range marks the beginning of the glass transition. Here, the behavior of the liquid starts to deviate from the one of the equilibrium liquid (indicated by the dashed black line in the upper panel of Fig. S7). The point where this departure from the equilibrium liquid occurs is highly dependent on the timescale of the experiment, i.e., dependent on the cooling rate in the transformation range. A fast-cooled liquid (1) falls out of equilibrium at higher temperatures (grey lines in the upper panel of Fig. S7) whereas a slow-cooled one (2) deviates from equilibrium liquid at lower temperatures (black lines in the same panel). That is, the glass transition has a kinetic component. The end of the transformation range is reached once relaxation times are so high that there is virtually no relaxation on the experimental timescale. Ultimately, this results in immobilized, glass-like behavior.

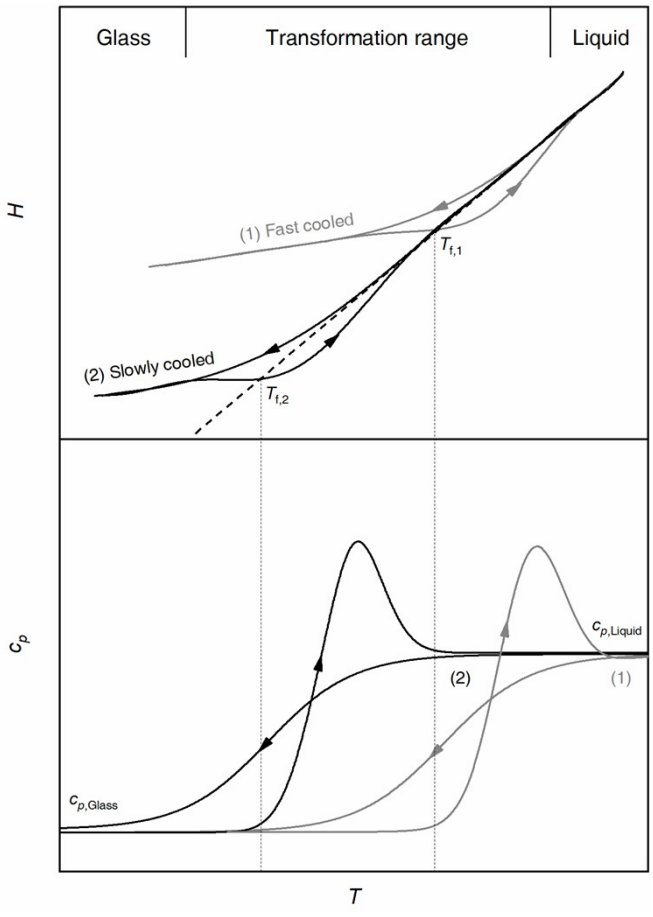

Figure S7. Schematic representation of enthalpy H and heat capacity c_p vs. temperature T when cooling and reheating a liquid at high (1) and slow (2) rate without crystallization.

Upon reheating the glass, relaxation becomes gradually faster until the system achieves equilibrium again. However, glasses hardly follow the same path as the one undertaken by the liquid upon cooling. This is because the mechanisms for relaxation in many systems are rather complex and can involve high activation energies. Consequently, higher temperatures are required for relaxation towards equilibrium to take place upon reheating. This relaxation delay is then overcompensated once the relaxation processes are finally enabled and the system "jumps" into equilibrium.

As enthalpy is a quantity that cannot be determined directly, experimentalists resort to measure its derivate, the isobaric heat capacity. This can easily be achieved via calorimetry measurements where the recorded heat flow is proportional to the heat capacity. The behavior of the heat capacity when cooling and heating through the glass transition is shown in the lower panel of Fig. S7. The transformation range is marked by a sigmoidal step-like drop in heat capacity that occurs at lower (higher) temperatures when employing a lower (higher) cooling rate. Upon reheating, the relaxation delay and subsequent overcompensation are manifested by a late but more abrupt increase in heat capacity, the so-called overshoot. That is, the overshoot is only observed upon reheating and not upon cooling. It becomes more pronounced if Q is low and the reheating rate high. Furthermore, it is dependent on specific properties of the liquid itself, i.e., the fragility (see next section), where more fragile liquids generally display larger overshoots than strong liquids.

3. The enthalpy differencing procedure by Wang et al.

In this section, we summarize concepts from the work of Wang, Velikov and Angell[3] that were used to determine the steepness indices m for the aqueous ionic liquids shown in Fig. 3b, c of the main manuscript. For further information (including a detailed set of references) please see this original publication.

Measures of fragility such as m are used to understand relaxation processes in the liquid and are especially useful when approaching the glass transition (see, e.g., the prominent review by Angell[5] and references therein). Fragility in general describes the deviation of relaxation behavior of liquids from Arrhenius behavior – high fragility thus indicates strong non-Arrhenius behavior and usually involves complex relaxation processes with high activation energies. The relaxation processes that govern fragility in liquids are not straightforward, which entails that the field largely relies on empirical datasets. Notably, the key advantage of the Wang et al. method is that it allows estimating (thermodynamic) fragility of glass-forming liquids out of simple calorimetry measurements.

Since m is defined as the Arrhenius slope at T_g, the following exponential relation is assumed

$$Q = Q_0 \exp\left[-\frac{E_g}{RT_g}\right] \tag{1}$$

where E_g is the activation energy for relaxation and T_g the glass transition temperature. E_g corresponds to the slope obtained from linear fitting in a $\ln(Q)$ vs. $1/T_g$ plot. That is, it is linked to the steepness index m via:

$$m = \frac{E_g}{ln10\ RT_g} \tag{2}$$

When comparing each rate Q to one fixed standard rate Q_S, eq. 1 can be rewritten as

$$ln\left(\frac{Q}{Q_S}\right) = \frac{E_g}{R}\left(\frac{1}{T_{g,S}} - \frac{1}{T_g}\right) = \frac{E_g}{RT_{g,S}}\left(1 - \frac{T_{g,S}}{T_g}\right) \quad (3)$$

and ultimately, inserting eq. 2 into eq. 3 yields:

$$log\left(\frac{Q}{Q_S}\right) = m - m\frac{T_{g,S}}{T_g} \quad (4)$$

That is, m can be extracted from the cooling rate dependence of the glass transition temperature. In order to minimize instrument error, the fictive temperature T_f is used as the value for the glass transition temperature T_g. It is defined as the temperature where the enthalpy of glass and liquid are identical, and is thus dependent on the cooling rate. In Fig. S7 the fictive temperatures of a fast- ($T_{f,1}$) and a slowly-cooled ($T_{f,2}$) glass are delineated. T_f is commonly evaluated using a rather tedious enthalpy conservation construction. Wang et al.[3] and Yue et al.[6] demonstrated independently from each other that T_f can also be evaluated for only one cooling rate and the T_fs for other rates can then be estimated using an enthalpy differencing procedure. This method requires cooling with varying rates (preferably with Q over several orders of magnitude) and warming with a single rate (e.g., 30 K min^{-1} as in our case). The thermodynamic basis of the procedure can easily be derived from Fig. S7 (upper panel): The fast-cooled glass not only exhibits a higher T_f but also a higher enthalpy than the slowly cooled one. The enthalpy change of each liquid upon vitrification can be expressed as

$$\Delta H = \int_{T_0}^{T_f} c_p dT \quad (5)$$

where c_p is the difference in heat capacity between the supercooled liquid and the glass, and T_0 is an arbitrary temperature in the equilibrium liquid state. Consequently, when assuming that c_p is temperature-independent in this narrow temperature range, the difference between the enthalpy of glass 1 (fast cooled) and glass 2 (slowly cooled) amounts to:

$$\Delta H' = \Delta H_2 - \Delta H_1 = c_{p,1}(T_{f,2} - T_0) - c_{p,2}(T_{f,1} - T_0) \quad (6)$$

If we suppose that $c_{p,1}$ and $c_{p,2}$ are identical, we obtain:

$$\Delta H' = c_p(T_{f,2} - T_{f,1}) \quad (7)$$

That is, the difference in enthalpy between the two glasses is directly proportional to the difference in fictive temperature. If we know $\Delta H'$ and c_p, we only need to determine the fictive temperature $T_{f,S}$ for one single cooling rate (the "standard rate" as mentioned above) in order to calculate T_f for all employed cooling rates. All can be extracted quickly from calorimetry traces, which will be demonstrated again using our scans from the benchmark glassformer glycerol.

Fig. S8 (left) shows calorimetry warming scans of glycerol with 30 K min^{-1} after quenching with rates ranging from 100 to 2 K min^{-1}. Heat flow is easily converted into heat capacity. It is evident that the heat capacity of glass and liquid is rather constant and largely independent of the employed cooling rate. Hence, the heat capacity difference c_p between supercooled liquid and glass can be read out from any heating curve.

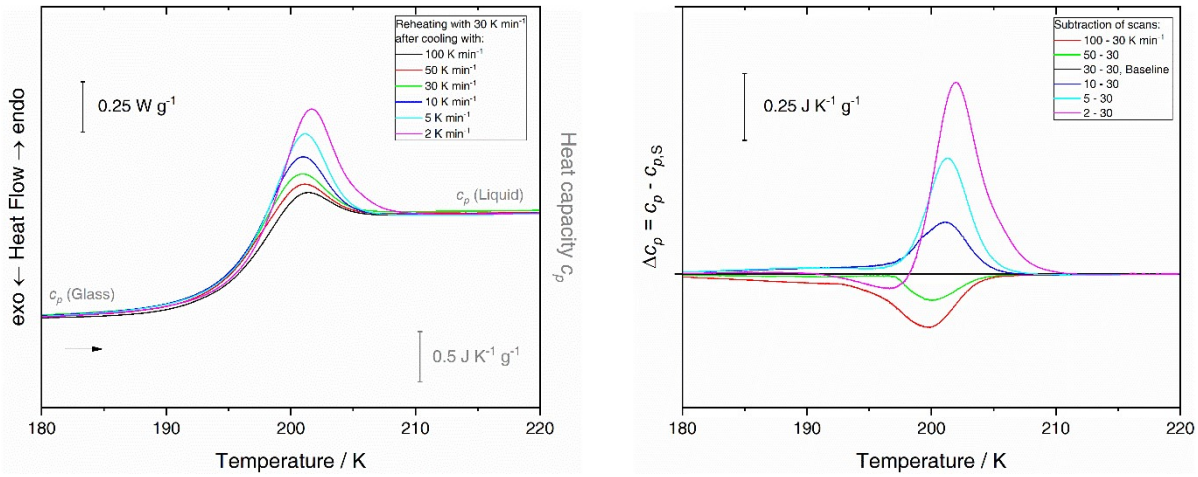

Figure S8. Left: Calorimetry reheating scans (30 K min^{-1}) of glycerol that was vitrified using rates between 100 and 2 K min^{-1}. Right: The same calorimetry traces after subtracting the standard scan (Q_S = 30 K min^{-1}).

$\Delta H'$, i.e., the excess enthalpy between the standard glass (cooled with Q_S) and the other glasses cooled with Q is obtained by (i) generating the difference between their heat capacity curves, and (ii) integrating them by temperature. In other words, the excess enthalpy is calculated from the difference in heat capacity overshoots. We chose 30 K min^{-1} as the standard cooling rate for two reasons: (i) It is identical to our used heating rate, and (ii) for this rate, T_f corresponds approximately to the onset temperature of the glass transition upon reheating. The result of the differencing procedure is shown in Fig. S8 (right). After integration, the area $\Delta H'$ for each subtracted cooling rate Q is inserted into eq. 7, alongside the other values (c_p, and T_f of the standard rate), yielding the fictive temperatures of all the glycerol glasses cooled at Q. Finally, following eq. 4, $\log(Q/Q_S)$ is plotted against $T_{f,S}/T_f$ (T_g is substituted by the more accurate T_f), and m is obtained via linear fitting (see Fig. S9).

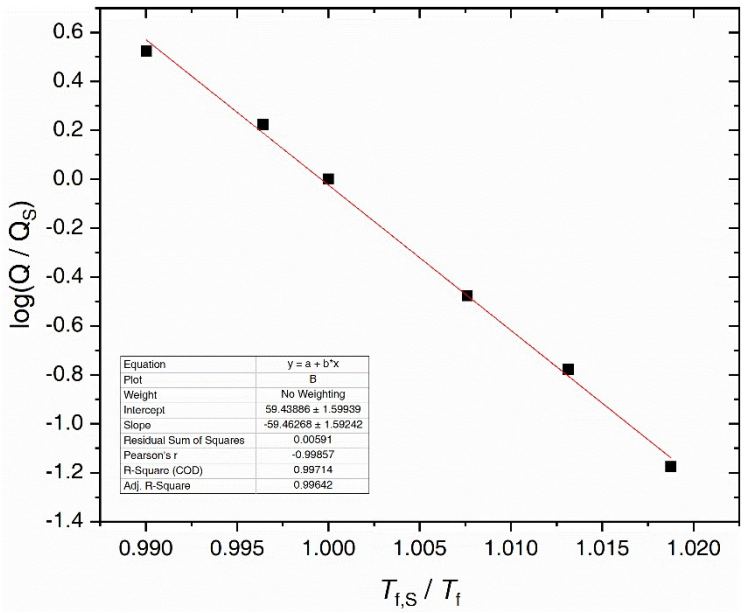

Figure S9. Arrhenius plot of cooling rate vs. resulting fictive temperature for pure glycerol. The plot is scaled by a fixed standard cooling rate of 30 K min^{-1} (y-Axis) and its corresponding standard fictive temperature (x-Axis). A linear fit of the data according to eq. 4 yields a value of m = 59.5 ± 1.6.

4. Overshoot behavior of aqueous ionic liquids used in this work

As demonstrated in the earlier sections, the overshoot behavior is an important trait that can be linked directly to excess enthalpy of the produced glass (see Fig. S8) and even to the fragility of the glass-forming liquid (see Fig. S9). Thus, in this section, we show magnifications of calorimetry scans of our aqueous ionic liquids (Figs. S10-S16) that emphasize their individual overshoot behavior. Details are given in the captions of the respective figures. The Angell mix $N_2H_5^+TFA^-$ is omitted as it is shown already in the main manuscript (Fig. 3a).

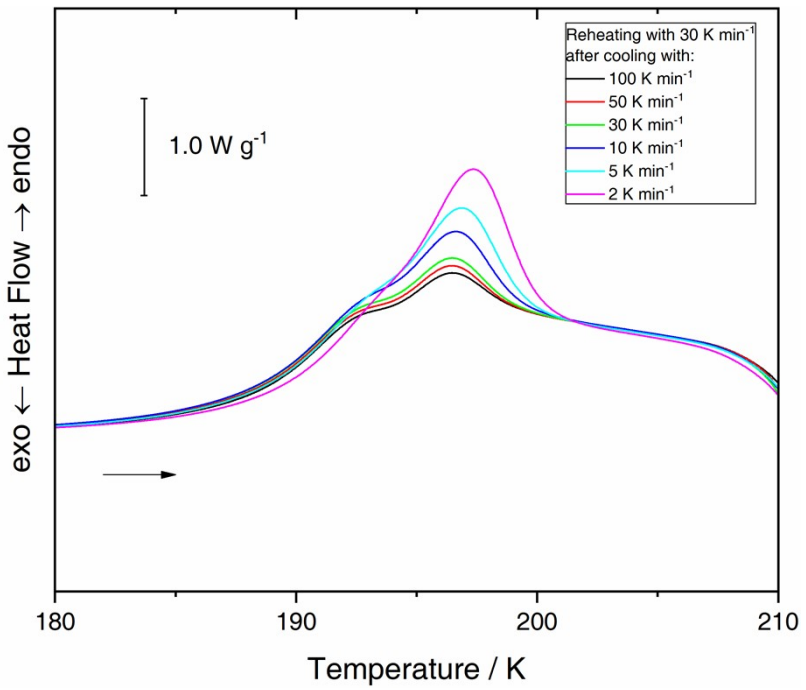

Figure S10. Calorimetry reheating scans (30 K min^{-1}) of aqueous $NH_4^+TFA^-$ (x = 0.175) that was cooled using rates between 100 and 2 K min^{-1}. Both parts of the asymmetric peak, the initial increase in heat capacity and endothermic bump, are affected by cooling rate. However, the endothermic bump is affected more considerably, which is why we assign it to the main overshoot feature of this glassy solution. Naturally, our estimate for m is mostly governed by this second feature. The occurrence of two endothermic steps (both with characteristics from overshoots) suggests that there there are two glass transitions that overlap with each other. This reinforces our argument of a phase-separated solution as outlined in the discussion part of the main manuscript.

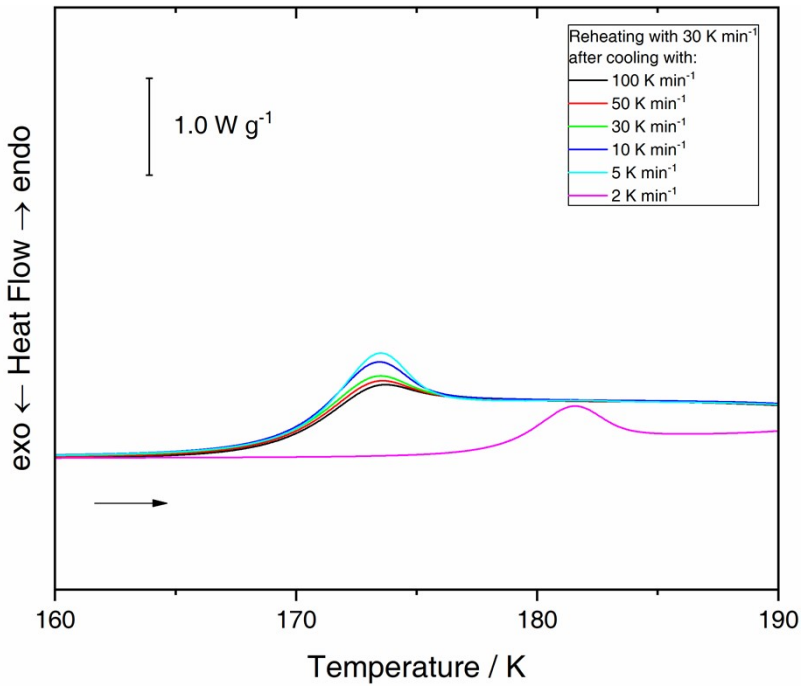

Figure S11. Calorimetry reheating scans (30 K min^{-1}) of aqueous $CH_3NH_3^+TFA^-$ (x = 0.175) that was cooled using rates between 100 and 2 K min^{-1}. Crystallization occurred upon cooling with 2 K min^{-1}, which is why this scan could not be used for the fragility plot in Fig. 3b of the main manuscript.

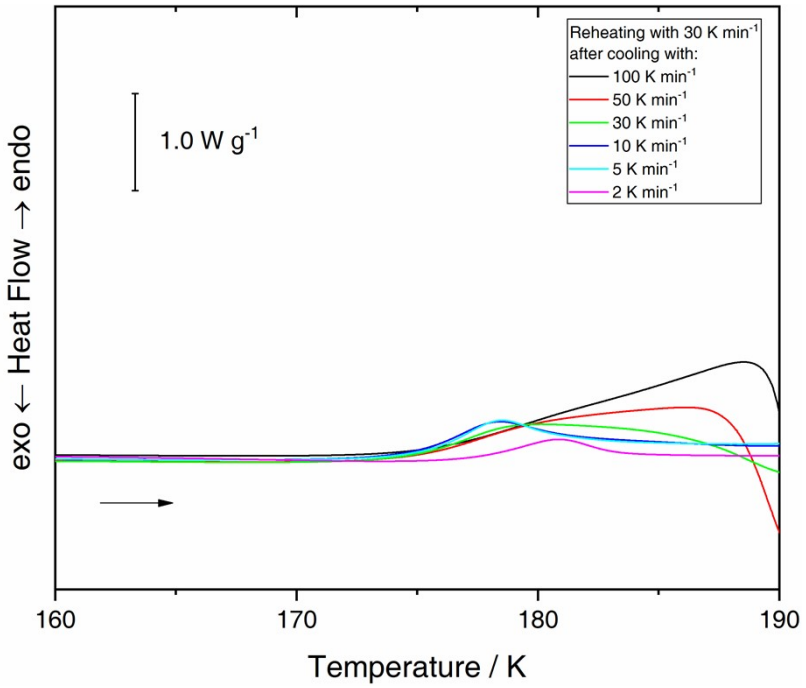

Figure S12. Calorimetry reheating scans (30 K min^{-1}) of aqueous $C_2H_5NH_3^+TFA^-$ (x = 0.175) that was cooled using rates between 100 and 2 K min^{-1}. The low-temperature exotherm upon cooling suddenly shifts to slightly higher temperatures when using a rate of 2 K min^{-1} (see Fig. S6). This indicates that crystallization most likely occurred, which is why this scan was not used for the fragility plot in Fig. 3b of the main manuscript. On first glance, there seems to be no typical overshoot behavior. Still, it is possible to extract enthalpy values via the differencing procedure. However, these scatter substantially due to the peculiar shape of the recorded calorimetry traces. This contributes significantly to the large error for m that is given in Fig. 3b.

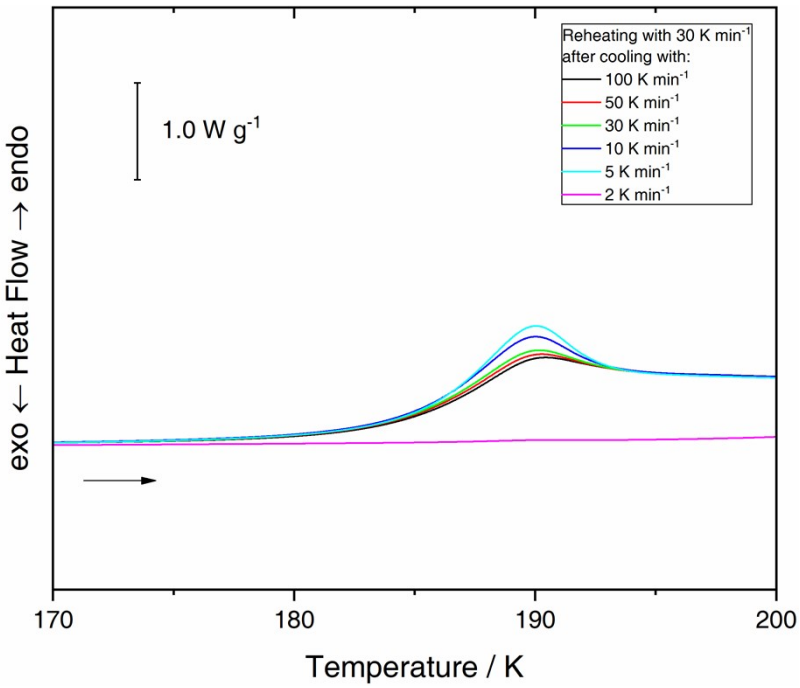

Figure S13. Calorimetry reheating scans (30 K min^{-1}) of aqueous $N_2H_5^+TCA^-$ (x = 0.175) that was cooled using rates between 100 and 2 K min^{-1}. Crystallization occurred upon cooling with 2 K min^{-1}, which is why this scan could not be used for the fragility plot in Fig. 3b of the main manuscript.

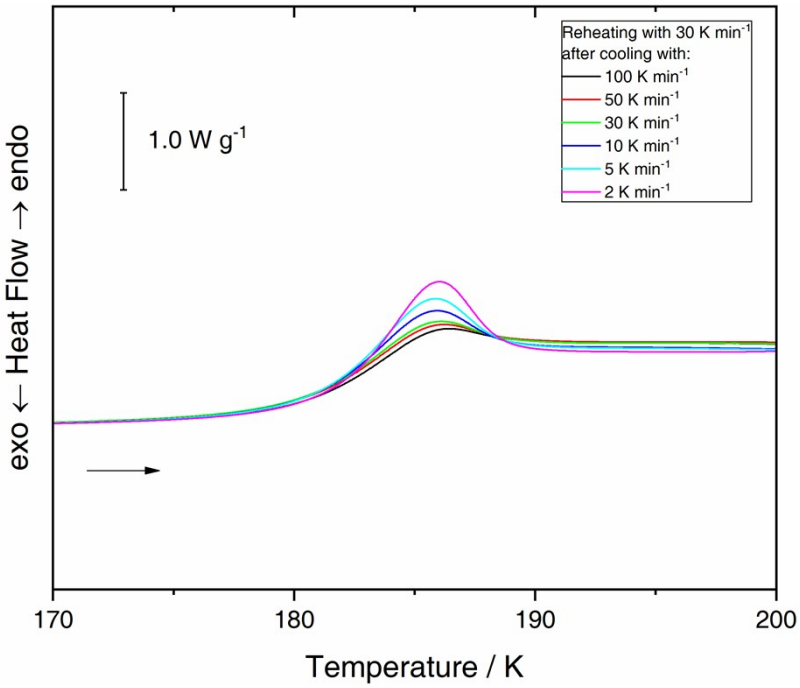

Figure S14. Calorimetry reheating scans (30 K min^{-1}) of aqueous $N_2H_5^+DCA^-$ (x = 0.175) that was cooled using rates between 100 and 2 K min^{-1}.

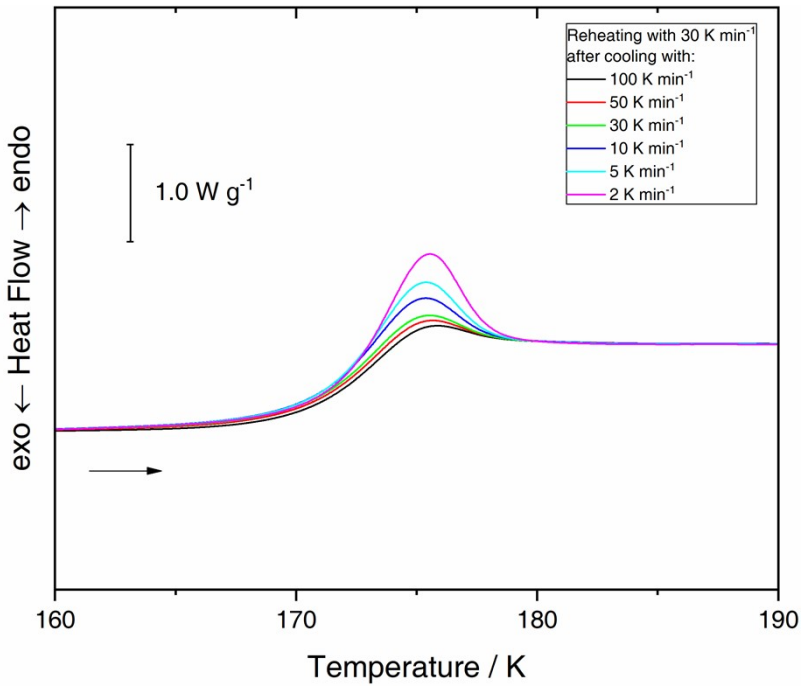

Figure S15. Calorimetry reheating scans (30 K min^{-1}) of aqueous $N_2H_5^+OAc^-$ (x = 0.175) that was cooled using rates between 100 and 2 K min^{-1}.

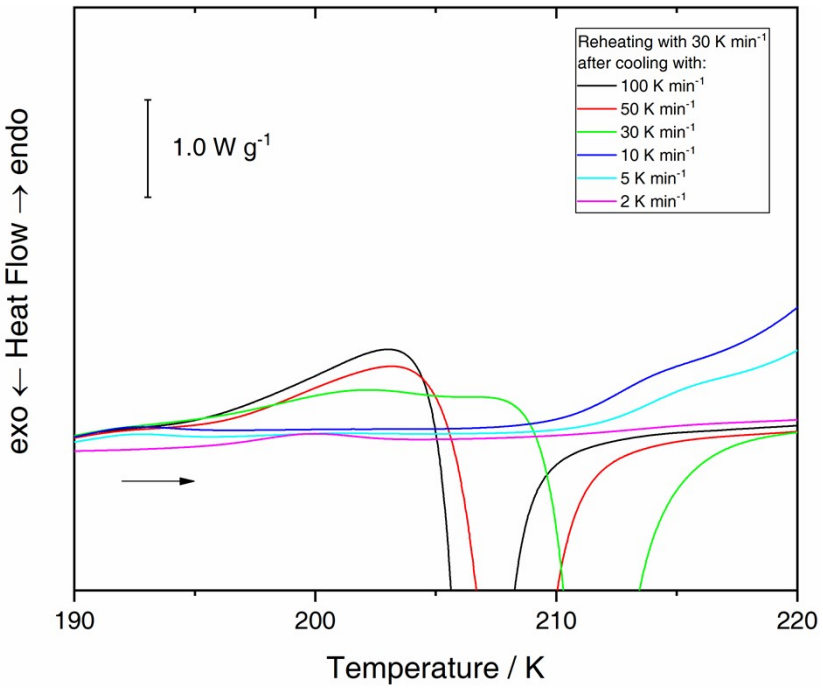

Figure S16. Calorimetry reheating scans (30 K min^{-1}) of aqueous $N_2H_5^+PFP^-$ (x = 0.175) that was cooled using rates between 100 and 2 K min^{-1}. The already rich phase behavior is heavily affected by the cooling rate. Here, it was not possible to extract somewhat sensible excess enthalpy values via the differencing procedure. This could be a sign that the variation of the endothermic features with cooling rate might not at all be due to the heat capacity overshoot.

5. Pair radial distribution functions, average hydrogen bond distances and average number of hydrogen bonds from MD simulation

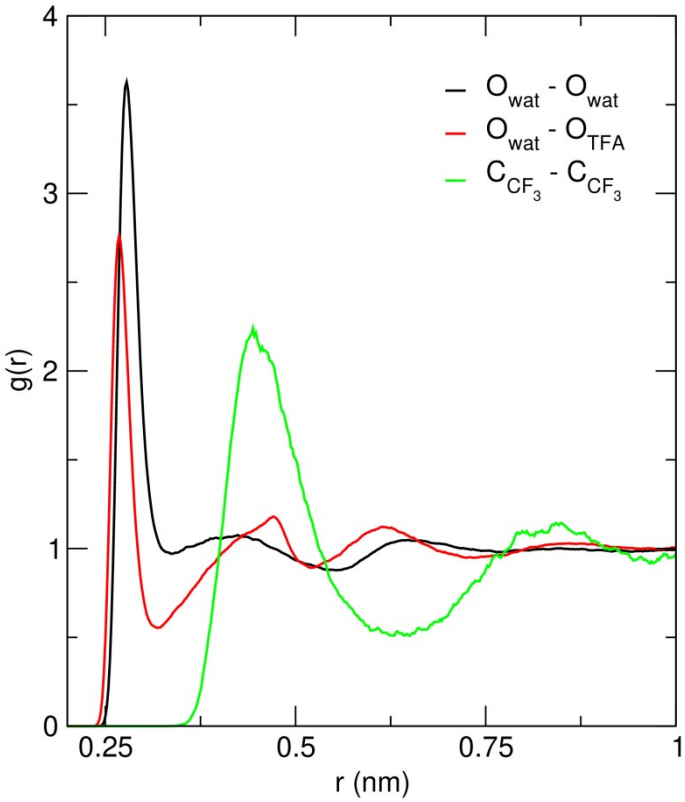

Figure S17. Pair radial distribution functions (g(r)) for the O···O contacts in water (black), the O_{wat}···O_{TFA} contacts (red) and the C···C contacts among CF_3 groups in TFA^-.

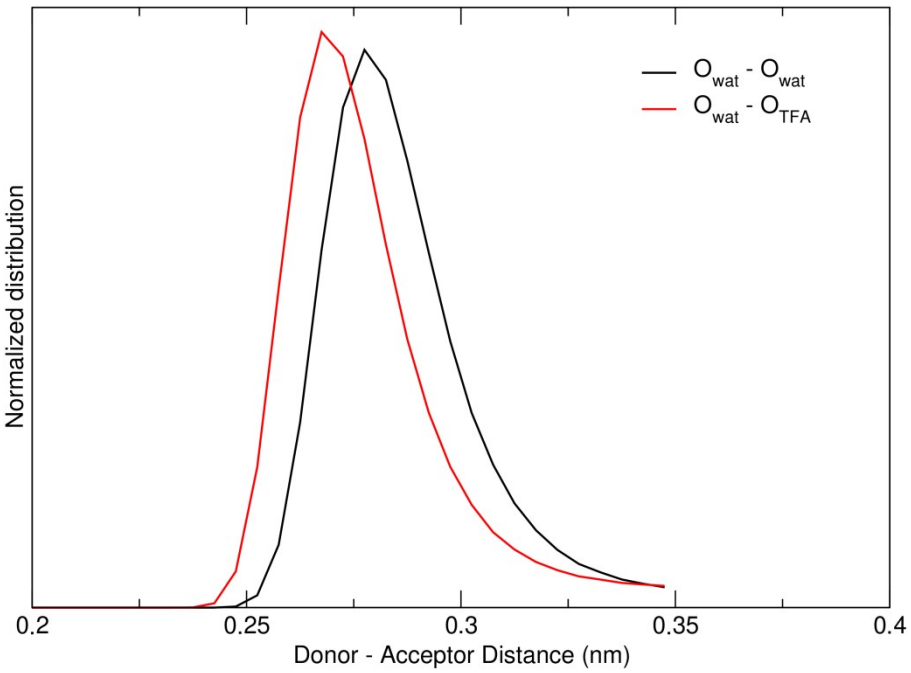

Figure S18. Normalized distribution of the donor–acceptor distance in the hydrogen bonds among water molecules (black) and between water and TFA^- (red).

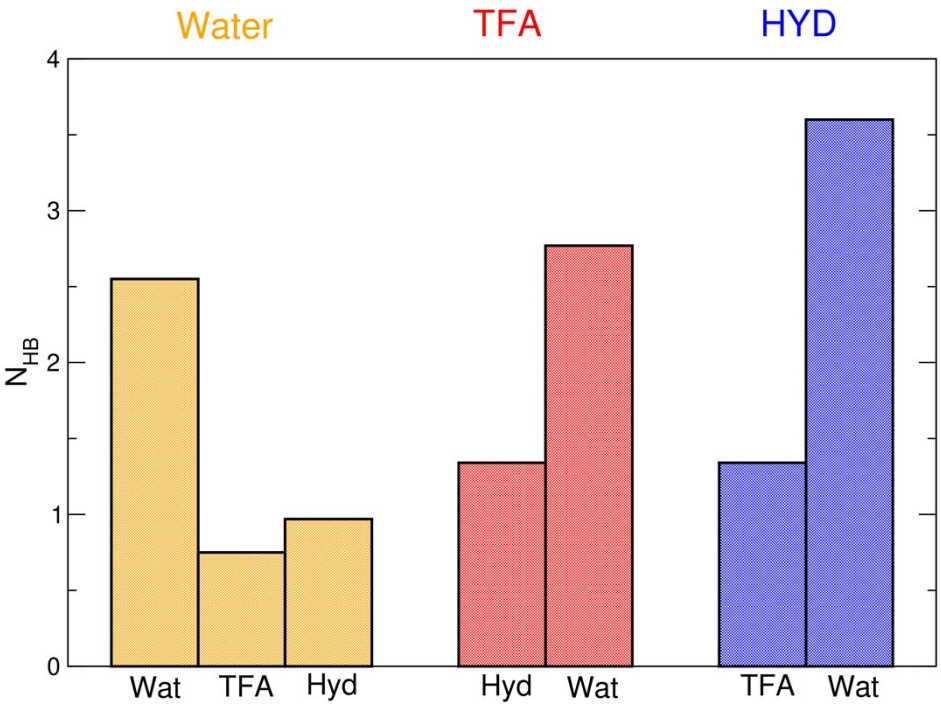

Figure 19. Analysis of the HB population along the MD simulation. The number of HB formed on average by each water molecule with water, TFA^- and $N_2H_5^+$ (here Hyd) is reported in orange. The number of HB formed on average by each TFA^- molecule with Hyd and water is reported in red. The number of HB formed on average by each Hyd molecule with TFA^- and water is reported in blue.

References

(1) Moynihan, C. T.; Easteal, A. J.; De Bolt, M. A.; Tucker, J. Dependence of the Fictive Temperature of Glass on Cooling Rate. *J. Am. Ceram. Soc.* **1976,** *59* (1-2), 12.

(2) Moynihan, C. T.; Easteal, A. J.; Wilder, J.; Tucker, J. Dependence of the glass transition temperature on heating and cooling rate. *J. Phys. Chem.* **1974,** *78* (26), 2673.

(3) Wang, L.-M.; Velikov, V.; Angell, C. A. Direct determination of kinetic fragility indices of glassforming liquids by differential scanning calorimetry: Kinetic versus thermodynamic fragilities. *J. Chem. Phys.* **2002,** *117* (22), 10184.

(4) Moynihan, C. T. Correlation between the Width of the Glass Transition Region and the Temperature Dependence of the Viscosity of High-Tg Glasses. *J. Am. Ceram. Soc.* **1993,** *76* (5), 1081.

(5) Angell, C. A. Liquid Fragility and the Glass Transition in Water and Aqueous Solutions. *Chem. Rev.* **2002,** *102* (8), 2627.

(6) Yue, Y. Z.; Christiansen, J. d.; Jensen, S. L. Determination of the fictive temperature for a hyperquenched glass. *Chem. Phys. Lett.* **2002,** *357* (1), 20.